REPORT

De Novo Missense Variants in *FBXW11* Cause Diverse Developmental Phenotypes Including Brain, Eye, and Digit Anomalies

Richard J. Holt,[1,26] Rodrigo M. Young,[2,3,26] Berta Crespo,[4,26] Fabiola Ceroni,[1,26] Cynthia J. Curry,[5] Emanuele Bellacchio,[6] Dorine A. Bax,[1] Andrea Ciolfi,[6] Marleen Simon,[7] Christina R. Fagerberg,[8] Ellen van Binsbergen,[7] Alessandro De Luca,[9] Luigi Memo,[10] William B. Dobyns,[11,12] Alaa Afif Mohammed,[13,14] Samuel J.H. Clokie,[13] Celia Zazo Seco,[15] Yong-Hui Jiang,[16] Kristina P. Sørensen,[8] Helle Andersen,[17] Jennifer Sullivan,[18] Zöe Powis,[19] Anna Chassevent,[20] Constance Smith-Hicks,[20] Slavé Petrovski,[21,22] Thalia Antoniadi,[13] Vandana Shashi,[18] Bruce D. Gelb,[23] Stephen W. Wilson,[2] Dianne Gerrelli,[4] Marco Tartaglia,[6] Nicolas Chassaing,[15,24] Patrick Calvas,[15,24] and Nicola K. Ragge[1,25,*]

The identification of genetic variants implicated in human developmental disorders has been revolutionized by second-generation sequencing combined with international pooling of cases. Here, we describe seven individuals who have diverse yet overlapping developmental anomalies, and who all have *de novo* missense *FBXW11* variants identified by whole exome or whole genome sequencing and not reported in the gnomAD database. Their phenotypes include striking neurodevelopmental, digital, jaw, and eye anomalies, and in one individual, features resembling Noonan syndrome, a condition caused by dysregulated RAS signaling. *FBXW11* encodes an F-box protein, part of the Skp1-cullin-F-box (SCF) ubiquitin ligase complex, involved in ubiquitination and proteasomal degradation and thus fundamental to many protein regulatory processes. FBXW11 targets include β-catenin and GLI transcription factors, key mediators of Wnt and Hh signaling, respectively, critical to digital, neurological, and eye development. Structural analyses indicate affected residues cluster at the surface of the loops of the substrate-binding domain of FBXW11, and the variants are predicted to destabilize the protein and/or its interactions. *In situ* hybridization studies on human and zebrafish embryonic tissues demonstrate *FBXW11* is expressed in the developing eye, brain, mandibular processes, and limb buds or pectoral fins. Knockdown of the zebrafish *FBXW11* orthologs *fbxw11a* and *fbxw11b* resulted in embryos with smaller, misshapen, and underdeveloped eyes and abnormal jaw and pectoral fin development. Our findings support the role of *FBXW11* in multiple developmental processes, including those involving the brain, eye, digits, and jaw.

Whole exome or whole genome sequencing (WES and WGS, respectively) has dramatically advanced the identification of genetic variants contributing to complex, rare, and clinically heterogeneous human disorders. However, because such variants might be private, it can be challenging to ascribe pathogenicity. Recently, WES and WGS and the international collation of affected individuals with variants in the same gene[1,2] have led to the identification of several developmental disorders. This approach, referred to as "reverse phenotyping," has been successfully applied to multiple intellectual disability syndromes, including those related to genetic variants in *FBXO11* (MIM: 607871),[3–5] and syndromes involving variants in *CDC42* (MIM: 116952) and *RAC1* (MIM: 602048),[6,7] all of which display clinical heterogeneity. Here, we use a similar approach to investigate the role of *de novo* variants in *FBXW11* (MIM: 605651) in human development.

[1]Faculty of Health and Life Sciences, Oxford Brookes University, Oxford OX3 0BP, UK; [2]Department of Cell and Developmental Biology, Biosciences, University College London, Gower St, London WC1E 6BT, UK; [3]Institute of Ophthalmology, University College London, 11-34 Bath Street, London EC1V 9EL, UK; [4]Great Ormond Street Institute of Child Health, University College London, London WC1N 1EH, UK; [5]Genetic Medicine, University of California, San Francisco/Fresno, Fresno, CA 93701, USA; [6]Genetics and Rare Diseases Research Division, Ospedale Pediatrico Bambino Gesù, Scientific Institute for Research, Hospitalization, and Healthcare, 00146 Rome, Italy; [7]Department of Genetics, University Medical Center Utrecht, 3508 GA Utrecht, the Netherlands; [8]Department of Clinical Genetics, Odense University Hospital, 5000 Odense C, Denmark; [9]Molecular Genetics Unit, Fondazione Casa Sollievo della Sofferenza, 71013 San Giovanni Rotondo, Italy; [10]Unità Operativa Complessa di Pediatria e Patologia Neonatale, Ospedale San Martino, 32100 Belluno, Italy; [11]University of Washington, Seattle, WA 98195-6320, USA; [12]Center for Integrative Brain Research, Seattle Children's Research Institute, Seattle WA 98101, USA; [13]West Midlands Regional Genetics Laboratory, Birmingham Women's and Children's National Health Service Foundation Trust, Mindelsohn Way, Edgbaston, Birmingham B15 2TG, UK; [14]Clinical and Chemical Pathology Department, Faculty of Medicine, Cairo University, 11562 Cairo, Egypt; [15]UDEAR, Université de Toulouse, UMRS 1056 Institut National de la Santé et de la Recherche Médicale-Université Paul Sabatier, 31059 Toulouse, France; [16]Department of Pediatrics and Neurobiology, Program in Genetics and Genomics, Duke University School of Medicine, Durham, NC 27710, USA; [17]Hans Christian Andersen Children's Hospital, Odense University Hospital, 5000 Odense C, Odense, Denmark; [18]Department of Pediatrics, Division of Medical Genetics, Duke University Medical Center, Durham, NC 27710, USA; [19]Department of Clinical Affairs, Ambry Genetics, Aliso Viejo, CA 92656, USA; [20]Department of Neurology, Division of Neurogenetics Kennedy Krieger Institute, Baltimore, MD 21205, USA; [21]Centre for Genomics Research, Discovery Sciences, Biopharmaceuticals R&D, AstraZeneca, Cambridge, CB4 0WG, UK; [22]Department of Medicine, the University of Melbourne, Melbourne, VIC 3010, Australia; [23]Mindich Child Health and Development Institute, Department of Pediatrics, and Department of Genetics and Genomic Sciences, Icahn School of Medicine at Mount Sinai, New York, NY 10029, USA; [24]Department of Medical Genetics, Purpan University Hospital, 31059 Toulouse, France; [25]West Midlands Regional Clinical Genetics Service and Birmingham Health Partners, Birmingham Women's and Children's National Health Service Foundation Trust, Birmingham, B15 2TG, UK
[26]These authors contributed equally to this work
*Correspondence: nragge@brookes.ac.uk
https://doi.org/10.1016/j.ajhg.2019.07.005.

Figure 1. Phenotypes of Individuals 1, 2, 4, 5, and 7

(A–C) Individual 1 at age 13 years, showing bilateral ptosis related to the underlying ocular anomalies (A), contractures affecting the distal interphalangeal joints of the left 4th and 5th fingers (B), and a wide sandal gap, short terminal phalanges, contractures affecting the 4th and 5th toes, 2–3 toe syndactyly, and scarring from surgery removing the left supernumerary toe (C).

(D–I) Individual 1 at age 24 years, showing bilateral microanterior segment and iris colobomas (D–G), contractures of the 4th and 5th left fingers (H), scarring from surgery removing the supernumerary toe, 2–3 toe syndactyly, and contractures of the 4th and 5th toes (I).

(legend continued on next page)

Through WES of 32 individuals with developmental eye anomalies, we identified a de novo missense variant (GenBank: NM_012300.2:c.1087C>T; NP_036432:p.Arg363Trp) in *FBXW11*. This variant was present in a girl with striking eye anomalies (bilateral microanterior segments, iris and chorioretinal coloboma, and lens anomalies), digital anomalies, and a psychiatric disorder (individual 1) (Figure 1, Tables 1 and S1, and the Supplemental Note). No other pathogenic variants were present in known eye development genes. Koolen et al.[8] previously described a boy with holoprosencephaly (HPE), seizures, small stature, preaxial polydactyly affecting the hand, "finger-like thumbs," and an increased sandal gap who had a de novo duplication encompassing seven genes, including *FBXW11*, on chromosome 5q35.1 (1.24 Mb). They hypothesized that his phenotype could be explained by the duplication of *FBXW11*, given its putative role in hedgehog (Hh) signaling and the phenotypic overlap with other disorders (HPE and polydactyly) caused by dysregulation of this pathway. Furthermore, duplication of the homologous gene *BTRC* (MIM: 603482) is implicated in split hand-foot malformation.[9] Moreover, FBXW11 participates in the Wnt/β-catenin signaling pathway,[10,11] which is fundamentally important in eye and brain development[12,13] and digit patterning.[14]

Through GeneMatcher,[2] we identified six other individuals with de novo missense variants in *FBXW11*; all were predicted to be damaging and found by WES or WGS. Five individuals (individuals 2–6) exhibited neurodevelopmental and/or digit anomalies, and one (individual 7) had a complex phenotype including brain anomalies and features suggestive of Noonan syndrome (Tables 1 and S1, Figure 1, and the Supplemental Note). Individual 7 had no pathogenic variants in genes currently included in Noonan syndrome or related RASopathy diagnostic panels. All genetic testing was performed under research ethics approval from the UK "Genetics of Eye and Brain anomalies" study (REC 04/Q0104/129), French (CPP Sud-Ouest and Outre-Mer II), American (Duke University, Pro00032301 - Genomic Study of Medical, Developmental, or Congenital Problems of Unknown Etiology), and Italian (Ospedale Pediatrico Bambino Gesù study 1702_OPBG_2018) ethics committees or by clinical diagnostic consent (Supplemental Material and Methods).

Our seven individuals presented with a range of overlapping phenotypes. Neurodevelopmental features commonly included neurodevelopmental delay (6/7), speech delay (5/7), autistic and/or stereotypical behaviors (3/7), psychiatric features (4/7), and micro- (1/7) or macrocephaly (3/7). MRI data from five individuals indicated corpus callosal hypoplasia (2/5), dilated ventricles (2/5), and white matter atrophy (2/5). Five of seven individuals had an under- or overdeveloped jaw. Digital anomalies were striking and included brachydactyly or short distal phalanges (3/7), polysyndactyly (2/7), widened interdigital spaces and/or sandal gap (2/7), camptodactyly or contractures (2/7), and underdeveloped thenar musculature (2/7). Individual 7 was clinically diagnosed with Noonan syndrome, and pulmonary stenosis, a recurrent feature of this disorder, was present in individual 5. Only individual 1 had developmental eye anomalies. Certain of these phenotypes overlap with those of the boy, presented by Koolen et al.,[8] who exhibited multiple digital anomalies, neurodevelopmental delay, and absence of the anterior part of the corpus callosum. From the published images, it also appears that he has broad halluces and short terminal phalanges. The latter are interesting because individual 4 had bilateral shortening of the thumbs and big toes, individuals 2, 4, and 7 had short terminal phalanges and/or brachydactyly, and individuals 2 and 4 had underdevelopment of the thenar eminence, akin to "finger-like thumbs." Although overlapping features can be seen, there is phenotypic diversity, which appears to be an emerging pattern for variants affecting genes controlling multiple cellular pathways and developmental processes; these gene include, for example, *CDC42*,[6] *FBXO11*,[3–5] *SHH* (MIM: 600725),[15,16] and *SOX2* (MIM: 184429).[17,18]

FBXW11 belongs to a highly conserved group of around 60 proteins characterized by a motif of ~40 amino acids (the F-box). This family is subdivided into three classes: FBXWs containing WD40 repeats, FBXLs containing leucine-rich repeats, and FBXOs containing either different protein-protein interaction modules or no recognizable motifs.[19] WD40-repeats are also a motif of approximately

(J–O) Individual 2 at age 9 years, showing a prominent nasal tip, broad columella, and retrognathia (J–K), the feet showing contractures (see the detailed view of the left 2nd toe), short distal digits, widely spaced toes, left 2–3 toe syndactyly, right 2nd toe clinodactyly (L and M) comparable to that of Individual 1, and MRI scans revealing an abnormal corpus callosum, an absent splenium, thick Probst bundles, small globular dysplastic hippocampi, and mildly reduced white matter volume (N and O).

(P–W) Individual 4 at age 18 years, showing dysmorphic facial features including mild ptosis of the upper eyelids, malar hypoplasia, a long and smooth philtrum, a bifid nasal tip, a thin upper lip (P), micrognathia, a tall sloping forehead, and small ears (Q); digital anomalies include shortening of the distal phalanx of the thumbs, 5th finger clinodactyly (R–U), thenar hypoplasia on the right (S), and mild thenar hypoplasia on the left (U); digital anomalies of the feet include shortening of the distal phalanx of the toes and increased convexity of all toenails (V and W).

(X–AB) Individual 5 at 4 months, showing a small chin (X), adducted thumbs not well shown as they are held by the clinician (Y and Z), and normal feet (AA and AB).

(AC) Individual 7 at 3 years and 2 months, showing frontal bossing; a deep, broad nasal bridge, epicanthus; low-set, posteriorly rotated ears; and a large, protruding tongue.

(AD–AJ) Individual 7 at 9 years and 8 months, showing frontal bossing; a deep, broad nasal bridge; epicanthus; low-set, posteriorly rotated ears (AD and AE); mild prognathism (AE); pectus carinatum (AF); and bilateral clinodactyly of the 4th and 5th toes (AG and AH). Brain MRI of Individual 7 showed complete agenesis of the corpus callosum with only a small residual portion of the anterior genum, a retro-cerebellar arachnoidal cyst (AI), and colpocephaly characterized by dilated lateral ventricles, specifically in the occipital and temporal horns and the third ventricle (AJ).

Table 1. Summary of Phenotypic and Genotypic Data of Individuals with *FBXW11* Missense Variants

Individual		1	2	3	4	5	6	7	Koolen et al. 2006[8]
Variant (GenBank: NM_012300.2; NP_036432.2)		c.1087C>T (p.Arg363Trp)	c.1091C>A (p.Ala364Asp)	c.1093G>A (p.Ala365Thr)	c.1330G>A (p.Glu444Lys)	c.1340G>A (p.Arg447Gln)	c.1340G>T (p.Arg447Leu)	c.724G>C (p.Gly242Arg)	1.24Mb duplication
gnomAD[26] frequency		absent	absent	absent	absent	absent	absent	absent	N/A
Inheritance		*de novo*	*de novo*	*de novo*	*de novo*	*de novo*	*de novo*	*de novo*	*de novo*
InterVar[77] classification		likely pathogenic	likely pathogenic	likely pathogenic	likely pathogenic	likely pathogenic	likely pathogenic	likely pathogenic	N/A
SIFT[78] classification		damaging	tolerated	damaging	damaging	damaging	tolerated	damaging	N/A
PolyPhen-2[79] classification		probably damaging	probably damaging	probably damaging	possibly damaging	probably damaging	probably damaging	probably damaging	N/A
Sex		female	male	male	female	female	male	male	male
Birth parameters	Term (weeks [+days])	40 (+5)	40	40 (+2)	39	40 (+6)	38	38	N/A
	Weight (kg)	4.08	3.63	3.95	3.15	3.17	3.40	3.22	N/A
Growth parameters (age)	Current age (years)	24	9	27	18	1	8	9 years, 7 months	19
	Weight in kg (%ile)	54 (34th %)	33.2 (79th %)	75 (68th %)	37.5 (0.1st %; −3.7 SD)	6.2 (0.1st %; −3.5 SD)	30.2 (82nd %)	24.5 (8th %)	N/A
	Height in cm (%ile)	169 (81st %)	138.4 (81st %)	180 (68th %)	146.2 (0.5th %; −2.5 SD)	66 (2nd %; −2.1 SD)	134.5 (86th %)	123.5 (2nd %; −2.1 SD)	157 (5.5th %) (at 15 years)
	Head circumference in cm (%ile)	58.4 (>99th %; +3.7 SD)	53 (64th %)	55.5 (61st %)	48.5 (<1st %; −5.5 SD)[a]	N/A	57 (>99th %; +3.5 SD)	56 (99th %)	57 (92nd %) (at 15 years)

(Continued on next page)

Table 1. Continued

Individual		1	2	3	4	5	6	7	Koolen et al. 2006[8]
Congenital anomalies	Facial	yes	yes	no	yes	yes	yes	yes	yes
	Mandibular	retrognathia	retrognathia	no	micrognathia	retrognathia	no	mild prognathism	no
	Ocular	bilateral microanterior segment, lens anomalies and colobomas, R microphthalmia	severe strabismus	mild myopia	no	alternating exotropia	no	mild myopia	no
	Hand	contractures of the 4th and 5th fingers	thinning of R and L thenar musculature, short 5th metacarpal, R transverse palmar crease, and relative brachydactyly	no	thinning of thenar musculature R > L and short distal phalanges of thumbs, bilateral mild 5th finger clinodactyly	no[b]	no	brachydactyly, small hands	right preaxial polydactyly, finger-like thumbs
	Foot	L middle toe polydactyly, wide sandal gaps, 2–3 toe syndactyly, contractures of the L 4th and 5th toes	mild 2–3 toe syndactyly, 2nd toe clinodactyly, brachydactyly, wide toe spacing, contractures of the 2nd and 4th toes, short 5th metatarsal	no	short terminal phalanges, wide sandal gaps	no	no	bilateral clinodactyly of the 4th and 5th toes, brachydactyly, small feet	wide sandal gaps
	Cardiac	no	no	no	no	pulmonary stenosis	no	patent foramen ovale	ventricular septal defect
	renal or urological	no	no	no	no	R renal hypoplasia	no	no	VUR
	Skeletal	no	no	no	yes	no	no	yes	no
Development	Motor delay	no	moderate	moderate	severe	severe	mild to moderate	severe	yes
	Intellectual deficiency	no	moderate to severe	severe	severe	delayed milestones	moderate to severe	moderate to severe	mild
	Speech and language delay	no	severe	severe	severe	N/A	moderate	moderate	N/A
Behavior	ASD or psychiatric features	psychiatric issues	repetitive behaviors	classic autism	hand stereotypy, self-injurious, impulsive and aggressive behavior	N/A	ASD, anxiety	self-injurious, impulsive and aggressive behavior	N/A

(*Continued on next page*)

Table 1. *Continued*

Individual		1	2	3	4	5	6	7	Koolen et al. 2006[8]
Neurological features	Tone	normal	increased	increased	narrow based gait	cerebral palsy	low	low	increased
	Seizures or EEG activity	N/A	mild slowing of cerebral activity	normal	N/A	N/A	N/A	normal	infrequent seizures
	MRI	N/A	hypoplasia of the corpus callosum, reduced white matter, abnormal hippocampi	N/A	normal	generalized white matter atrophy, periventricular white matter changes with ischemic damage	mild prominence of lateral ventricles	hypoplasia of the corpus callosum, mild prominence of lateral ventricles	lobar HPE, hypoplasia of the corpus callosum
Other relevant findings		none	umbilical and inguinal hernias	none	hyperkinetic	circulatory collapse at few days of age	dermal melanosis, cupped ears	webbed neck, bilateral cryptorchidism	N/A

Details of the previously reported individual with the 1.24Mb duplication[8] are included in a separate column for reference. Detailed information is provided in the Supplemental Note and Table S1. The protein domains are reported according to UniProt annotations. All variants are absent from gnomAD. Variant locations are given according to GenBank: NM_012300.2 and NP_036432.2. Clinical interpretation of genetic variants according to ACMG/AMP 2015 guidelines was automatically predicted by InterVar for missense variants. Where available, information regarding inheritance was included in the InterVar prediction. Abbreviations are as follows: ASD = autism spectrum disorder; L = left; N/A = not available; R = right; and VUR = vesicoureteric reflux.
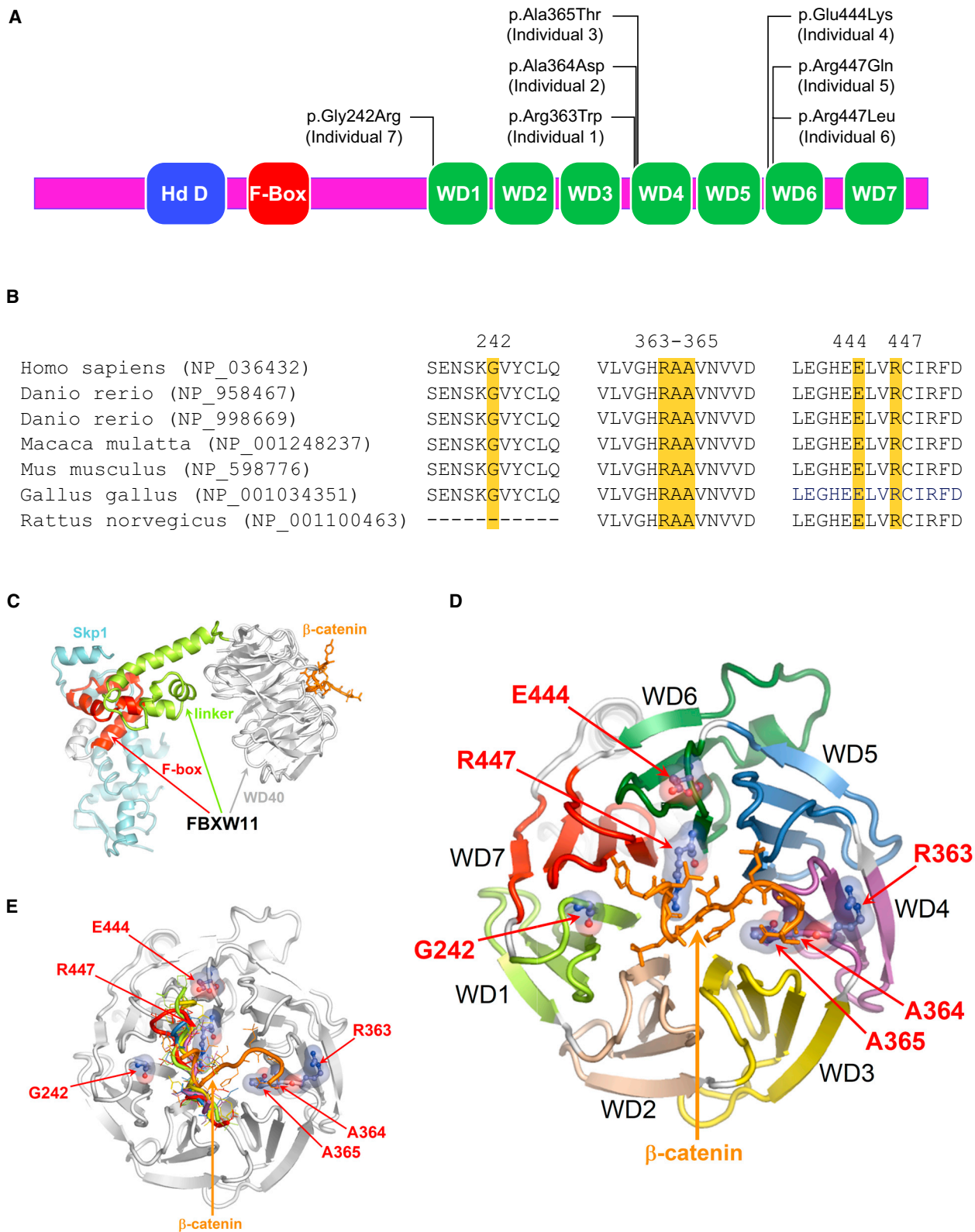[a]Extreme microcephaly.
[b]Adducted thumbs.

Figure 2. Structural Modeling of *FBXW11* Missense Variants

(A) A schematic representation of FBXW11 showing the relative locations of the homodimerization domain D (Hd D, blue), F-box (red), WD40 domains (green), and the missense variants identified in our seven individuals.

(B) A Clustal Omega alignment of the FBXW11 regions containing the variants identified in this study showing affected amino acids highlighted in yellow and complete conservation across species.

(C) A homology model of FBXW11 in complex with Skp1 and β-catenin based on PDB structure PDB: 1P22. Skp1 is shown in blue, β-catenin in orange, and the FBXW11 domains in red (F-box), green (linker region), and gray (WD40 domains).

(legend continued on next page)

Table 2. FoldX Predictions of the Impact on FBXW11 and BTRC Stability and Their Interactions with Skp1 and β-catenin of the *FBXW11* Variants Identified in Individuals 1–7

Individual			1	2	3	4	5	6	7
Variant			p.Arg363Trp	p.Ala364Asp	p.Ala365Thr	p.Glu444Lys	p.Arg447Gln	p.Arg447Leu	p.Gly242Arg
FBXW11	FBXW11	ΔΔG	0.521609	4.09086	4.12764	−0.0159721	1.63651	0.1246	12.0844
		Stability	minor decrease	decrease	decrease	none	decrease	none	decrease
	+ Skp1	ΔΔG	0.0	0.0	0.482	0.0	0.0	0.9022	9.6142
		Stability	none	none	minor decrease	none	none	minor decrease	decrease
	+ β-catenin	ΔΔG	0.12782	4.943962	3.866386	−0.37936	2.2931	1.55266	10.19112
		Stability	none	decrease	decrease	none	decrease	decrease	decrease
BTRC	BTRC	ΔΔG	0.51728	4.47495	3.59842	−0.10002	1.54555	0.0186672	10.264
		Stability	minor decrease	decrease	decrease	none	decrease	none	decrease
	+ Skp1	ΔΔG	0.0	0.0	0.6572	0.0	0.0	0.7318	8.8664
		Stability	none	none	minor decrease	none	none	minor decrease	decrease
	+ β-catenin	ΔΔG	0.14382	5.78723	3.457756	−0.33198	2.279382	1.5214	9.16596
		Stability	none	decrease	decrease	none	decrease	decrease	decrease

ΔΔG provided as kcal mol^{-1}. Values of ΔΔG greater than 0.46 kcal mol^{-1} indicate a decrease in stability, whereas decreases greater than −0.46 kcal mol^{-1} indicate an increase in stability. Mean values of ΔΔG for five replicate analyses of each variant are given.

40 amino acids and typically fold into a β-propeller structure that is involved in protein-protein interaction.[20,21] Alterations in other F-box genes, for example *FBXO11*[3–5] and *FBXL4* (MIM: 605654), have been associated with neurodevelopmental disorders.[22] FBXW11 is a substrate adaptor of the Skp1-cullin-F-box (SCF) ubiquitin ligase complex, which catalyzes phosphorylation-dependent ubiquitination.[11,23] It has several targets, including β-catenin and GLI transcription factors, key mediators of the Wnt and the Hh pathways, respectively. Despite the importance of these two pathways, little is known about the role of *FBXW11* in human development and the impact of aberrant FBXW11 function on human disease.

Different *in silico* metrics indicate that *FBXW11* is moderately intolerant to variation.[24,25] It has a Residual Variation Intolerance Score (RVIS) of −0.47, ranking it among the 23% of human protein-coding genes most intolerant to functional (missense, nonsense, and splice) variants.[24] Moreover, metrics reported on gnomAD (v2.1.1)[26] suggest it is intolerant to both loss-of-function (LoF) variants (observed/expected [o/e] score = 0.15, 0.08–0.31 90% confidence interval [CI]; pLI score = 0.98) and missense variants (o/e score = 0.37, 0.32–0.43 90% CI; Z score = 3.96). The latter is of particular relevance because all the *de novo* variants in this study are missense changes. In addition to these seven variants, two further *de novo* changes of uncertain clinical significance in *FBXW11* have been reported in large scale studies of autism spectrum disorder (ASD) (GenBank: NM_012300.2:c.243C>G [p.Asp81Glu];

dbSNP: rs995419585, c.508C>T [p.Arg170Ter]).[27,28] None of these nine variants or other changes affecting these amino acids were listed on gnomAD, with the exception of a rare synonymous variant for Ala365 (dbSNP: rs775168567, GenBank: NM_012300.2:c.1095C>T, minor allele frequency [MAF] = 0.00001771) and a missense change for Arg170 (dbSNP: rs995419585, GenBank: NM_012300.2:c.508C>G [p.Arg170Gly], MAF = 0.000003984). Furthermore, the nucleotide positions affected by our seven missense variants are evolutionarily conserved according to the GERP rejected substitutions scores[29,30] (Table S1). Interestingly, these variants are located in regions depleted for nonsynonymous variation (Figure S1). According to the model developed by Havrilla et al.,[31] six of the seven missense changes affect residues located within portions of the protein considered as under the highest constraint in the human genome, ranking among the top 5% constrained coding regions (CCRs). The amino acid substitution (c.724G>C [p.Gly242Arg]) in individual 7, who presented with features of Noonan syndrome, is located in a region characterized by a slightly lower level of constraint (85th percentile). Therefore, the location of the variants in these regions further supports their potential relevance to protein function.

Intriguingly, all seven missense variants affected the WD40 domain of FBXW11 (Figure 2). In particular, six of the seven changes appeared to cluster at the N-terminal end of the WD4 (residues 363 to 365, in individuals 1, 2, and 3, affecting consecutive amino acids) and WD6 (residues 444 and 447, in individuals 4, 5, and 6 [individuals

(D) The locations of the amino acids affected by the *FBXW11* variants within the WD40 domain. β-catenin is shown in orange.
(E) The modeled WD40 domain of FBXW11 in complex with β-catenin (orange) and other available peptides known to bind FBXW7 or Cdc4 (cyclin E C-terminal degron, cyclin E N-terminal degron, DISC1, high-affinity CPD phosphopeptide from human cyclin E, SIC1).
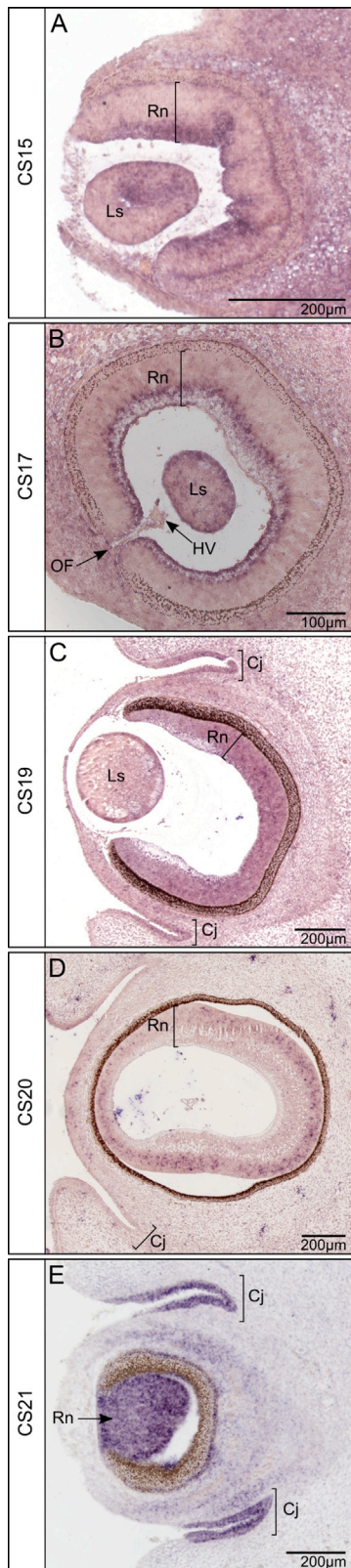
Figure 3. *In Situ* Hybridization Studies Showing *FBXW11* Expression During Human Eye Development

(A–E) Sagittal sections of the eye at CS15 (A), CS17 (B), CS19 (C), CS20 (D), and CS21 (E) made by using the 5′ UTR probe showing a strong *FBXW11* signal in the lens (A–C), the retina (A–E), the lips of the optic fissure closure (B), and regions of the developing conjunctiva (C and E). As eye development progresses, the stronger

5 and 6 had the same affected amino acid]) repeats. The seventh variant (in individual 7) affected the N-terminal end of the WD1 repeat. In contrast with this specific distribution, the two variants reported in the ASD-affected individuals[27,28] either affected a different domain of FBXW11 (p.Asp81Glu, homodimerization domain), or resulted in a truncated, likely inactive, protein (p.Arg170Ter).

No protein structure for FBXW11 was available in the Research Collaboratory for Structural Bioinformatics Protein Data Bank (RCSB PDB).[32] However, an experimentally derived crystal structure for a homolog, BTRC, complexed with Skp1 and β-catenin was available (PDB: 1P22).[20] Pairwise alignment of BTRC (GenBank: NP_003930.1) and FBXW11 (GenBank: NP_036432.2) show the proteins have 79.0% identity and 87.4% similarity, and the regions containing the missense variants in individuals 1–7 were highly conserved (Figure S2). Therefore, we modeled a 3D structure for FBXW11 (GenBank: NP_036432.2) based on the crystal structure of BTRC, employing a previously described procedure.[33] The location of the affected residues was visualized with PyMOL v2.0 (the PyMOL Molecular Graphics System, Version 2.0 Schrödinger). Notably, all affected residues were located toward the tips of the loops of the WD repeat domains, which are predicted to mediate substrate binding (Figure 2). Because there is high conservation of the WD repeat structure, and because each repeat contacts β-catenin,[20] all seven altered residues are expected to impact substrate binding. Clustering of the *de novo* missense variants suggests an impact on protein function via gain-of-function or dominant-negative mechanisms.[34] Despite this, and the fact that the phenotypes of these individuals fall in broad, overlapping categories, there is variation in the specifics of their features. We modeled the WD40 domain of FBXW11 bound to substrates of the WD40-domain-containing proteins FBXW7 and Cdc4 (Figure 2E). This indicated that individual substrates might adopt different orientations when binding to FBXW11, suggesting a variable contribution of the different WD40 motifs in FBXW11 binding to individual ligands. Therefore, it is possible that the missense variants identified here might have varying impacts depending on the substrate.

We investigated the impact of the missense variants on protein stability and interaction with Skp1 and β-catenin for both our modeled FBXW11 structure and BTRC by using FoldX.[35] Predictions indicated five of the seven missense variants (c.1087C>T [p.Arg363Trp]; c.1091C>A [p.Ala364Asp]; c.1093G>A [p.Ala365Thr]; c.1340G>A [p.Arg447Gln]; and c.724G>C [p.Gly242Arg]) impact the stability of both FBXW11 and BTRC (Table 2). Furthermore, five of the variants (p.Ala364Asp, p.Ala365Thr, p.Arg447Gln, p.Arg447Leu, and p.Gly242Arg) were predicted to decrease the stability of the FBXW11-β-catenin and BTRC-β-catenin

signal observed in the retina progressively shifts from the inner toward the outer retinal layers (A–D). Abbreviations are as follows: Cj = conjunctiva; HV = hyaloid vasculature; Ls = lens; OF = optic fissure; and Rn = retina.
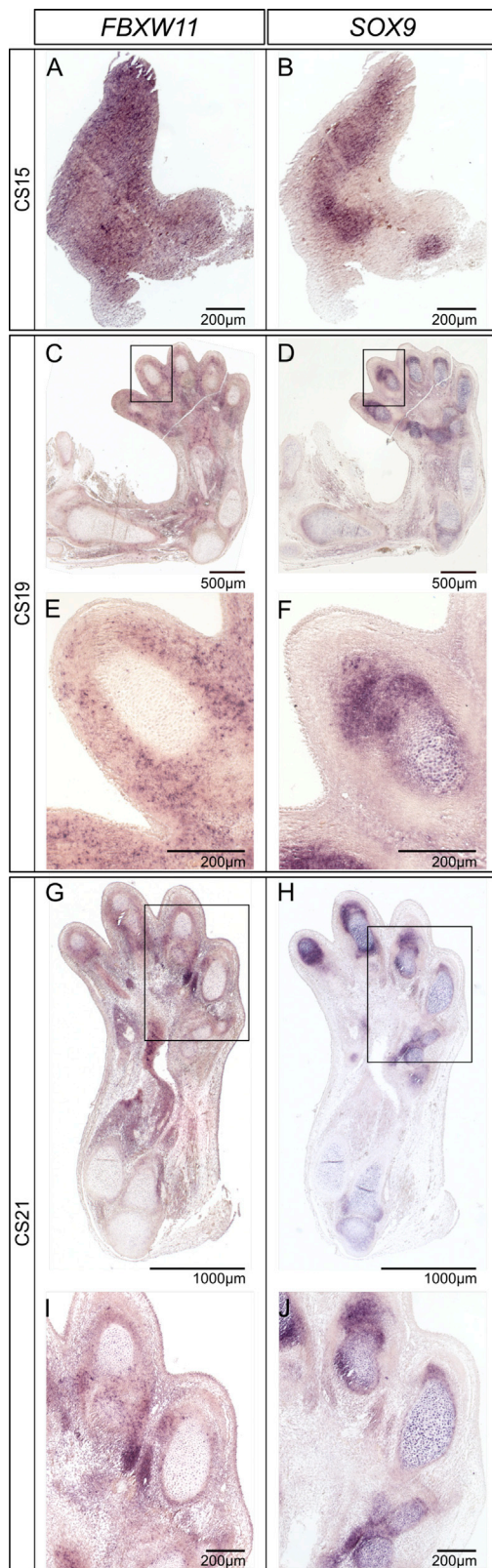
Figure 4. *In Situ* **Hybridization Studies Comparing** *FBXW11* **and**
SOX9 **Expression During Human Limb Development**
(A–J) Coronal sections of the forelimb at different CS
stages showing the expression pattern of *FBXW11* (5′ UTR
probe) on the left (A, C, E, G, and I) and the chondrogenic
marker *SOX9* on the right (B, D, F, H, and J). E, F, I, and
J show increased magnification of the boxed regions at CS19

interactions. Three variants (p.Ala365Thr, p.Arg447Leu, and
p.Gly242Arg) also decreased the stability of the FBXW11-
Skp1 and BTRC-Skp1 interactions (Table 2). Interestingly,
the variant (p.Gly242Arg) in individual 7, who presented
with features of Noonan syndrome, was predicted to have
the greatest impact on both FBXW11 and BTRC stability
and their interactions with β-catenin and Skp1. On the basis
of these analyses, the variants are predicted to produce vari-
able downstream effects and resultant phenotypes, particu-
larly because FBXW11 is involved in multiple developmental
pathways.

Next, we determined the expression profile of *FBXW11*
during human development by using nonradioactive RNA
in situ hybridization on human embryo sections from Car-
negie Stages (CS) 15–21, obtained from the MRC/Wellcome
Trust Human Developmental Biology Resource, UCL,
with full ethical approval.[36] We designed two probes to
target all three *FBXW11* human isoforms (GenBank:
NM_012300, NM_033644, and NM_033645) (Supple-
mental Material and Methods). Both probes showed similar
expression patterns (Figures 3–5 and S3–S6).

In the eye, *FBXW11* expression was seen throughout
the lens at multiple time points (Figures 3A–3C, S3A–
S3F, S3I, and S3J), a fact of particular relevance to the
congenitally absent and thin lenses in individual 1. In
the retina, *FBXW11* expression appeared to shift over
time from the inner to outer neuroretinal cell layers (Fig-
ures 3A–3D). Sagittal sections of the eye at CS17 also
showed *FBXW11* expression at the margins of the optic
fissure (Figures 3B, S3C, and S3D), indicating a potential
role in optic fissure closure, relevant to the bilateral
chorioretinal colobomas in individual 1. Expression of
FBXW11 was also seen in the developing conjunctiva
(Figures 3C, 3E, and S3E–S3J).

In the developing hand, expression of *FBXW11* was
analyzed in parallel with expression of the chondrogenic
marker *SOX9* (MIM: 608160).[37] At CS15, a strong signal
was detected for both genes (Figures 4A, 4B, S4A, and
S4B); *FBXW11* displayed more widespread expression
throughout the limb bud compared with the restricted
expression pattern of *SOX9*. At CS19 and CS21, after the
digits have begun to form, strong *FBXW11* expression
was seen in the mesenchyme surrounding the developing
cartilage (Figures 4C–4J and S4C–S4J). Interestingly, digital
anomalies were observed in four of the individuals we
report, as well as the boy reported by Koolen et al.[8]

In the brain, *FBXW11* expression was present in the
primitive ventricles (CS17 and CS19, Figures 5A–5C, S5A,
S5B, S6A, and S6 B), metencephalon (CS19, Figures 5C,
S5B, and S6B), hypothalamus (CS17, Figure 5D), and me-
dulla (CS17, Figure 5E). These expression patterns are
consistent with the altered brain structure, including
prominence of the lateral ventricles and periventricular

(C and D) and CS21 (G and H) highlighting *FBXW11* expres-
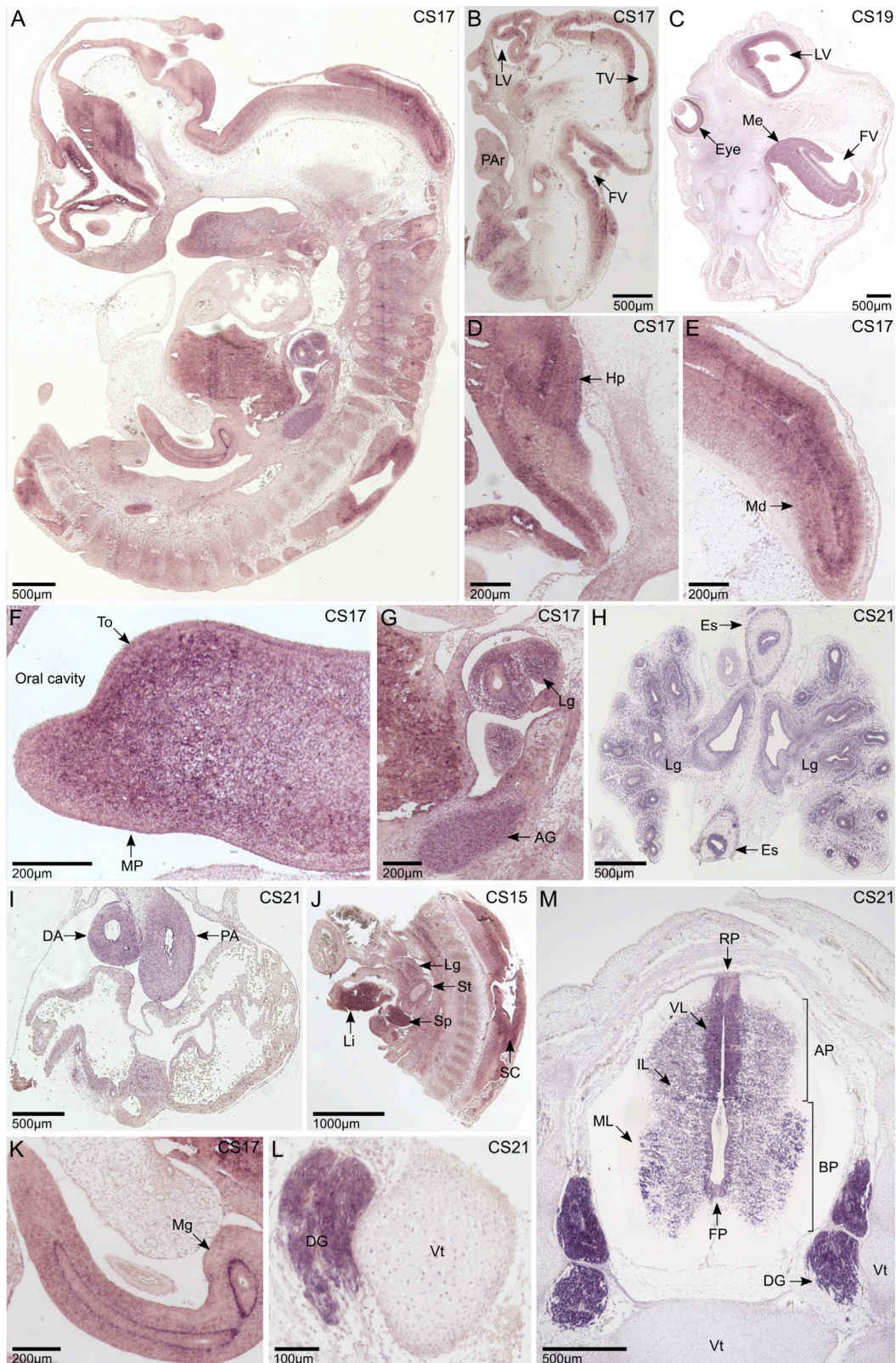sion around the developing cartilage of the digits in the hand
plate.

Figure 5. _In Situ_ Hybridization Studies of _FBXW11_ in the Human Showing the Expression Pattern in Multiple Structures during Embryonic Development

Experiments performed using the 5′ UTR probe. Structures of interest are indicated by arrows.

(A) A sagittal section of embryo at CS17 (week 6), showing _FBXW11_ expression in multiple developing structures.

(B) A sagittal section of the head at CS17 (week 6) indicating expression in the structures forming the lateral, third, and fourth ventricles.

(C) A sagittal section of the head at CS19 (week 7) showing strong expression in the regions surrounding the lateral ventricle and the metencephalon.

changes, of individuals 2, 5, 6, and 7. Furthermore, this finding supports an important role for FBXW11 in pathways, including the Hh and the Wnt cascades, essential for normal brain development.[38,39] Strong expression was also observed in the pharyngeal arches, including the mandibular process and tongue (CS17, Figures 5F, S5C, and S6C). Expression in these structures might relate to the micrognathia or retrognathia of four of the reported individuals (1, 2, 4, and 5) and the large tongue in individual 7. Other structures showing expression included: the adrenal glands (CS17, Figures 5G, S5D, and S6D), the lungs (CS17 and CS21, Figures 5G, 5H, S5E, and S6E), the pulmonary artery and dorsal aorta (CS21, Figures 5I, S5F, and S6F), the liver (CS15, Figures 5J, S5G, and S6G), the spleen (CS15, Figures 5J, S5G, and S6G), and the midgut (CS17, Figures 5K, S5H, and S6H); the dorsal ganglia (CS21, Figures 5L, S5I, and S6I) and the spinal cord (CS15, Figures 5J, S5G, and S6G; CS17 Figures 5A, S5A, and S6A; and CS21, Figures 5M, S5J, and S6J), where the signal was detected in the floor plate, the roof plate, and the ventricular and intermediate layers of the spinal cord (CS21, Figures 5M, S5J, and S6J). The expression in the pulmonary artery and dorsal aorta is interesting given the pulmonary stenosis seen in individual 5.

The zebrafish genome includes two orthologs of *FBXW11*, *fbxw11a* and *fbxw11b*. These genes encode proteins with 90.4% sequence identity and 95.3% similarity. Furthermore, both zebrafish orthologs share around 85% identity and 91% similarity with human FBXW11 (GenBank: NP_036432.2) (Fbxw11a [GenBank: NP_958467.1]: 84.7% identity, 90.6% similarity; Fbxw11b [GenBank: NP_998669.2]: 85.6% identity, 91.2% similarity). We performed *in situ* hybridization with probes designed against the low homology 3′ UTR region of *fbxw11a* and *fbxw11b* to avoid cross-detection (Supplemental Material and Methods).[40] At 4 days post fertilization (dpf), *fbxw11a* is expressed at low levels in the retina and brain and higher levels in the jaw mesenchyme (Figure 6A). *fbxw11b* is expressed widely in the brain and eyes, and there are high levels in the retinal ganglion layer, inner nuclear layer, in or adjacent to the outer plexiform layer, in the photoreceptor layer, ciliary marginal zone, jaw mesenchyme, oral epithelia (Figure 6B), and pectoral fins (Figures S7A–S7D). These findings are comparable to the expression

data in humans, further supporting a role for *FBXW11* in the development of the eye, jaw, limbs, and brain.

To further investigate the role of *FBXW11* in vertebrate development, we generated zebrafish knockdown models by using a combination of morpholino and CRISPR-Cas9 technologies (Supplemental Material and Methods). Morpholino knockdown of *fbxw11a* resulted in no overt phenotype in zebrafish embryos (Figures S7E and S7F). *fbxw11b* morphants consistently showed reduced eye size and a shorter and bent axis phenotype (Figures S7E and S7G). Because morpholinos can have off-target effects, using CRISPR-Cas9 we induced a 7bp frameshift mutation (allele u5010, p.Asp24Leufs*6) in *fbxw11b* exon 2 (Figures 6C and S7H–S7K). *fbxw11b*[u5010/u5010] homozygous embryos showed no abnormal phenotype and were viable and fertile. Maternal zygotic (MZ) mutant *fbxw11b*[u5010/u5010] embryos from an *fbxw11b*[u5010/u5010] female to *fbxw11b*[+/u5010] male cross also showed no abnormal phenotype (Figures 6D and 6E).

We hypothesized that compensation by *fbxw11a* could result in the absence of phenotype in MZ*fbxw11b*[u5010/u5010] embryos. For instance, recent studies have shown that the loss of function of a gene resulting from nonsense-mediated decay (NMD) might be compensated for by altered expression of other genes.[41–43] Because our CRISPR-Cas9 *fbxw11b* mutant carries a frameshift mutation, it might be subject to NMD. Therefore, the lack of phenotype observed might be a result of compensatory gene expression, possibly by *fbxw11a*. However, *in situ* hybridization experiments did not show any obvious upregulation of *fbxw11a* in *fbxw11b* mutants at 48 h post fertilization (hpf) (not shown). Therefore, the basal level of expression of *fbxw11a* might be sufficient to compensate for the lack of function of *fbxw11b*. To begin to address this issue, we injected *fbxw11a* morpholino (mo[fbxw11a]) in MZ*fbxw11b*[u5010/u5010] and sibling embryos. No overt phenotype was generated before 2dpf in any genotype, and no phenotype was observed in morpholino-injected heterozygous or wild-type siblings at any stage examined. By 3dpf, MZ*fbxw11b*[u5010/u5010]/mo[fbxw11a] morphants showed abnormally developed pectoral fins and heart edema (Figures 6D–6I, n = 20/21); this is of interest given the digital anomalies in the individuals presented here. At 5dpf, MZ*fbxw11b*[u5010/u5010]/mo[fbxw11a] morphant knockdown

(D–G) Increased magnification of structures from (A) highlighting *FBXW11* expression in the hypothalamus (D), lower medulla (E), pharyngeal arches (F), and the adrenal glands and lungs (G).

(H) A coronal section at CS21 (week 8) showing expression in the lungs.

(I) A coronal section of the heart at CS21 showing *FBXW11* expression in the dorsal aorta and the pulmonary artery.

(J) A sagittal section of the embryo at CS15 (week 5) highlighting strong *FBXW11* expression in the liver, spleen, and spinal cord.

(K) Increased magnification of (A) showing *FBXW11* expression in the midgut.

(L) A transverse section at CS21 showing a strong *FBXW11* signal in the dorsal ganglia.

(M) A transverse section of the spinal cord at CS21 showing *FBXW11* expression in the floor plate, roof plate, and the ventricular and the intermediate layers of the spinal cord.

Abbreviations are as follows: AG = adrenal glands; AP = alar plate; BP = basal plate; DA = dorsal aorta; DG = dorsal ganglia; Es = Esophagus; FP = floor plate; FV = fourth ventricle; Hp = hypothalamus; IL = intermediate layer; Lg = lungs; Li = liver; LV = lateral ventricle; Md = medulla; Me = metencephalon; Mg = midgut; ML = marginal layer; MP = mandibular process; PA = pulmonary artery; Par = pharyngeal arches; RP = roof plate; SC = spinal cord; Sp = spleen; St = stomach; To = tongue; TV = third ventricle; VL = ventricular layer; and Vt = vertebra.
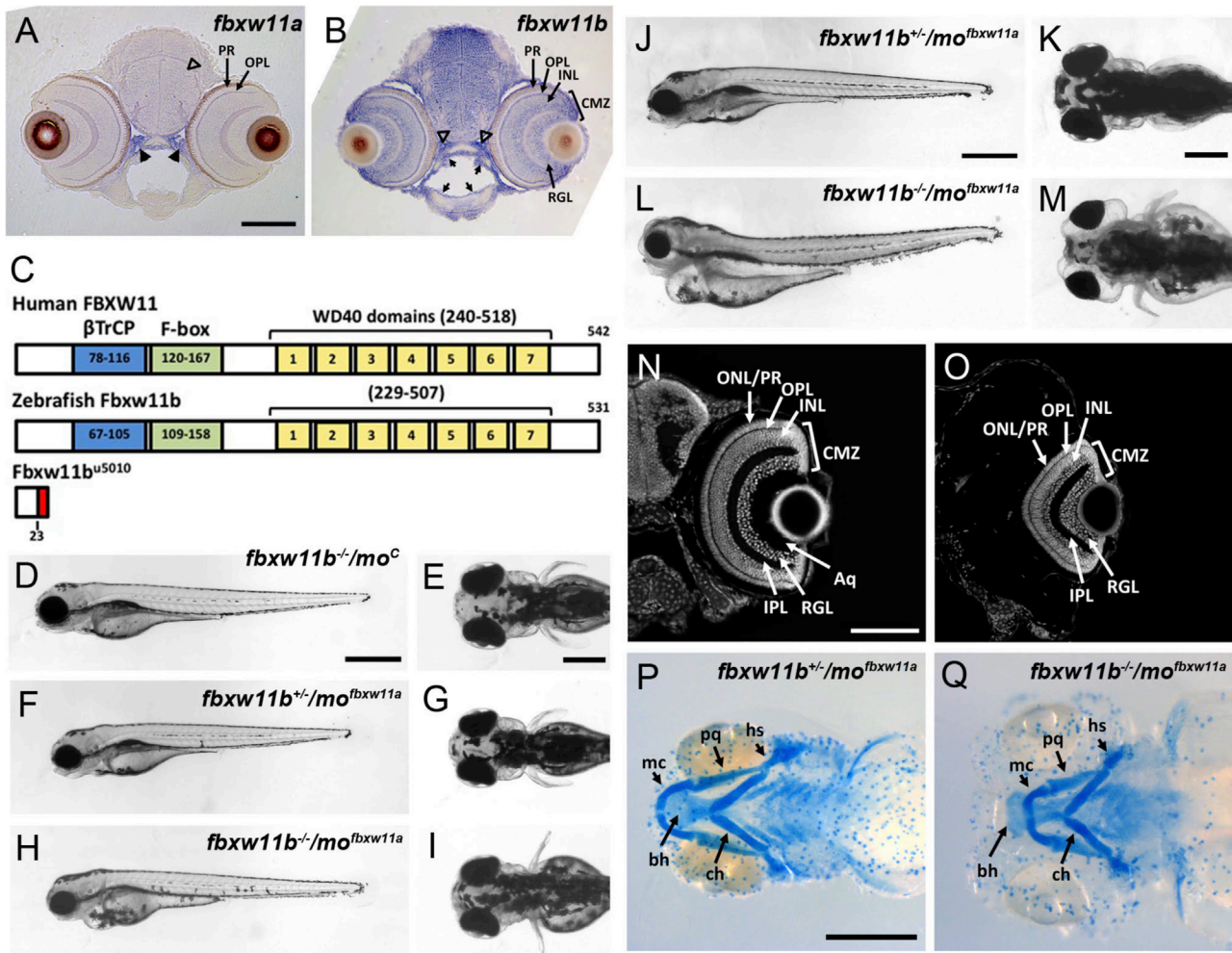
Figure 6. *fbxw11a* and *fbxw1b* Are Expressed in the Zebrafish Eye, and Their Knockdown Leads to Abnormal Eye and Jaw Development

(A and B) Coronal plastic sections showing the expression pattern of *fbxw11a* (A) and *fbxw11b* (B) in 4dpf zebrafish heads detected by *in situ* hybridization. Dorsal is up. The scale bar in (A) is 100μm.

(C) Diagram of human FBXW11 and zebrafish Fbxw11b and Fbxw11b[u5010]. The βTrCP domain is in blue, the F-box domain is in green, the seven WD40 domains are in yellow, and the nonsense sequence of Fbxw11b[u5010] is in red. The numbers are amino acid positions in respective proteins.

(D–I) 3dpf live zebrafish *MZfbxw11[u5010/u5010]* (D, E, H, and I) and *MZfbxw11b[+/u5010]* (F and G) embryos injected with 500pg of control (D and E) or *fbxw11a* (F–I) morpholinos. Lateral (D, F, and H) and dorsal (E, G, and I) view, both anterior to left. The scale bar in (D) is 400μm and in (E) is 200μm.

(J–Q) 5dpf zebrafish *MZfbxw11b[+/u5010]* (J, K, N, and P) and *MZfbxw11[u5010/u5010]* (L, M, O, and Q) embryos injected with 500pg *fbxw11a* morpholino. (J–M) Live embryos lateral (J and L) and dorsal (K and M) view, both anterior to left. The scale bar in (J) is 400μm and in (K) is 200μm.

(N and O) Confocal imaging of DAPI-stained coronal plastic sections. The scale bar in (N) is 100μm.

(P and Q) Alcian blue staining of cartilage structures. Ventral view, anterior to left. The scale bar in (P) is 200μm.

Abbreviations are as follows: Aq = aqueous humor; bh = basihyal; ch = ceratohyal; CMZ = ciliary marginal zone; hs = hyosymplectic; INL = inner nuclear layer; IPL = inner plexiform layer; mc = Meckel's cartilage; ONL = outer nuclear layer; OPL = outer plexiform layer; pq = palatoquadrate; PR = photoreceptor layer; and RGL, retina ganglion layer.

embryos developed periocular edema and smaller eyes compared to *MZfbxw11b[+/u5010]/mo[fbxw11a]* knockdown heterozygous siblings (Figures 6J–6M, n = 20/20). Coronal sections showed that 5dpf *MZfbxw11b[u5010/u5010]/mo[fbxw11a]* knockdown eyes had all the retinal layers present in the wild-type; however, the eye was smaller and misshapen. This was potentially because of a lack of aqueous humor in *MZfbxw11b[u5010/u5010]/mo[fbxw11a]* knockdowns, although it was present in the phenotypically normal siblings at the same stage (Figures 6N and 6O). The reduction

in eye size in mutant knockdown fish supports a role for *FBXW11* in eye development and supports the *FBXW11* variant's being implicated in the microphthalmia observed in individual 1. Alcian blue cartilage staining in *MZfbxw11b[u5010/u5010]/mo[fbxw11a]* knockdowns revealed abnormal development of the jaw (Figures 6P and 6Q). The basihyal (pharyngeal arch) cartilage structure protruded anteriorly in *MZfbxw11b[u5010/u5010]/mo[fbxw11a]* knockdowns because of shorter Meckel's and palatoquadrate cartilages (Figures 6P and 6Q). These latter observations are consistent

with four of our individuals presenting with retrognathia or micrognathia.

FBXW11 has been shown to negatively regulate the Wnt/β-catenin pathway.[44] Inhibition of Wnt/β-catenin signaling is required for the correct specification of forebrain territories, and enhanced Wnt activity leads to embryos with smaller or no eyes.[45,46] Enhanced Wnt activity in *tcf7l1a* mutants results in a smaller eye field and reduced eye size by 32hpf.[47] To determine whether Wnt/β-catenin signaling was affected in *fbxw11b*[u5010/u5010] embryos, we assessed whether there were any genetic interactions between the mutated forms of *fbxw11b* and *tcf7l1a*. As previously shown,[47] *tcf7l1a*^{−/−} eyes were close to 50% of the size of wild-type eyes (Figure S8A). However, *fbxw11b*[u5010/u5010]/ *tcf7l1a*^{−/−} double mutant embryos developed even smaller eyes, about 80% of the size of eyes in *tcf7l1a* embryos (Figure S8A, p = 0.0001, *tcf7l1a*^{−/−} embryos, $\tilde{x}$ = 910.337μm^3 ± 118e^3 n = 20; *fbxw11b*[u5010/u5010]/ *tcf7l1a*^{−/−} embryos, $\tilde{x}$ = 727.588 ± 145e,^{3} n = 19). This suggests that abrogation of *fbxw11b* leads to further enhanced Wnt signaling in *tcf7l1a*^{−/−} mutants. Furthermore, exposure of embryos to a low dose of the Wnt/β-catenin agonist BIO (0.5μm treatment from 24hpf onward) led to an upward bent trunk in *fbxw11b*[u5010/u5010]/*mo*[fbxw11a] knockdown embryos but not in *fbxw11b*[u5010/u501] or wild-type embryos (Figures S8B–S8D, 100% n = 13, two experiments). This morphology is similar to that observed in APC mutants in which the Wnt pathway is constitutively overactivated.[48] Overall, these results suggest that the *fbxw11b*[u5010/u5010]/*mo*[fbxw11a] knockdown embryos are sensitized to the effects of enhanced Wnt/β-catenin activity.

Given the phenotype of individual 1 and our *in situ* and zebrafish data, we further explored whether *FBXW11* variants contribute more widely to developmental eye disorders by performing targeted screening in an additional 263 individuals with anophthalmia, microphthalmia, or coloboma (AMC) by using high-resolution melt curve analysis[49] or Sanger sequencing (Supplemental Material and Methods). Excluding three 3′ UTR private variants (c.*4064_* 4065insT [chr5:171,288,698–171,288,699], c.*2867G>A [chr5:171,289,855], c.*2592C>T [chr5:171,290,168]; GenBank: NM_012300.2, GRCh37/hg19) inherited from unaffected parents, no functionally relevant variants were identified. Similarly, array comparative genome hybridization (aCGH) analysis of 77 individuals, including individual 1, with isolated or syndromic AMC did not identify any copy number aberrations affecting *FBXW11*. This indicates variants in *FBXW11* might only rarely be associated with human AMC.

FBXW11 is involved in multiple developmental pathways, including Wnt signaling, which plays a crucial role in the regulation of cell proliferation, tissue patterning, and organ morphogenesis. Wnt signaling can be divided into canonical and non-canonical pathways; and a key element of the former is ubiquitination of β-catenin (Figures S9A and S9B).[10,50] This ubiquitination, controlled by the SCF complex, is directed either by BTRC or its paralog BTRC2, encoded by *BTRC* and *FBXW11*, respectively.[11,51] Aberrations of this pathway can lead to a range of human pathologies, including developmental disorders affecting the limbs, as well as neurodevelopmental and psychiatric disorders.[10,52,53] There is also significant evidence of the importance of Wnt signaling in developmental eye disorders in mouse models.[54,55]

FBXW11 is also involved in Hh signaling by regulating the ubiquitination of GLI transcription factors (Figures S9C and S9D). Variants in Hh pathway genes are associated with developmental anomalies, some of which are comparable to those observed in the individuals presented here. Copy number gains encompassing *BTRC* are linked with developmental limb anomalies.[9,56] *Drosophila* with mutations in *Slimb*, the ortholog of both *FBXW11* and *BTRC*, develop supernumerary limbs or ectopic legs and eye anomalies.[57–59] In mice, mutations of GLI transcription factors can cause multiple malformations, including polydactyly, anophthalmia, and coloboma.[60–63] Finally, in humans, genetic variants affecting members of the Hh signaling pathway, such as *SHH* and *PTCH1* (MIM: 601309), have been associated with developmental eye anomalies and HPE.[15,64–66] *GLI2* (MIM: 165230) and *GLI3* (MIM: 165240) variants have also been reported in individuals with a variety of phenotypic features including HPE, polydactyly, and anophthalmia.[67–70] However, some of the *GLI2* variants have subsequently been classified as benign in ClinVar.

Individual 7 presented with distinctive characteristics of Noonan syndrome, a phenotype linked to RAS-MAPK signaling dysregulation.[71,72] Ras trafficking and activity are regulated by several mechanisms, including ubiquitination, which can be mediated by different ubiquitin ligase complexes.[73] Recent studies have also identified a circuit involving LZTR1, a Kelch-domain-containing protein altered in Noonan syndrome. LZRT1 functions as a substrate receptor in the cullin 3 ubiquitin ligase complex involved in the ubiquitination and functional down modulation of HRAS.[33,74,75] Interestingly, the SCF-β-TrCP E3 ligase complex has also been implicated in the ubiquitination and proteasomal degradation of HRAS,[76] supporting an unanticipated functional link between FBXW11 and RAS signaling modulation warranting further exploration.

Our structural analyses provide evidence of the specific impact of the identified variants on FBXW11 function, as well as for the dominant role of these amino acid changes. Specifically, the variants are predicted to impair proper recognition and/or binding of substrates by the SCF ubiquitin ligase complex. In contrast to the presently reported variants, the two *de novo* changes previously reported in the ASD-affected individuals are predicted to alter protein function by different mechanisms. The exon 3 missense variant is located within the homodimerization domain and might interfere with protein dimerization. Instead, the nonsense substitution affecting exon 4 is predicted to lead to NMD or a truncated protein, potentially reducing the amount of functional protein. Although several of

our individuals presented with features of ASD, little clinical information is available for the individuals from these ASD studies, except that the individual carrying the nonsense variant has a high IQ.[28] This limits our ability to suggest further how these alternate mechanisms might contribute to phenotypic variation.

In conclusion, we report seven unrelated individuals presenting with phenotypes including eye, digital, and jaw anomalies, and neurodevelopmental or psychiatric disorders. These individuals all carry *de novo* probably pathogenic missense variants in *FBXW11*, a member of the ubiquitin ligase SCF complex that functions as a regulator of both the Wnt and Hh signaling developmental pathways. *In silico* analyses provide a model for the functional impact of the variants; *in vitro* experiments with human and zebrafish developmental tissue supported early expression of *FBXW11* in relevant structures and *in vivo* zebrafish studies documented the relevance of FBXW11 in developmental processes affected in this phenotypic series. Collectively, these data support the role of *FBXW11* variants in human developmental disorders affecting the brain, eye, jaw, and digits, possibly via modulation of the Wnt/β-catenin, Hh, and RAS signaling pathways.

Supplemental Data

Supplemental Data can be found online at https://doi.org/10.1016/j.ajhg.2019.07.005.

Declaration of Interests

Zöe Powis was an employee of Ambry Genetics. Slavé Petrovski is Vice-president and Head of Genome Analytics for AstraZeneca Centre for Genomics Research (CGR), Cambridge, UK.

Web Resources

Allen Brain Atlas, https://www.brain-map.org/
ANNOVAR, http://annovar.openbioinformatics.org/
CCR Browser, https://s3.us-east-2.amazonaws.com/ccrs/ccr.html
ClinVar, https://www.ncbi.nlm.nih.gov/clinvar/
EMBOSS Needle, https://www.ebi.ac.uk/Tools/psa/emboss_needle/
ExAC, http://exac.broadinstitute.org/
GeneMatcher, https://genematcher.org/
gnomAD, https://gnomad.broadinstitute.org/
InterVar, http://wintervar.wglab.org/
OMIM, https://www.omim.org/
Picard, http://broadinstitute.github.io/picard/index.html
POVRay, www.povray.org/
PyMOL, https://pymol.org/2/
RCSB Protein Data Bank, www.rcsb.org
UCSC Genome Browser, https://genome.ucsc.edu/
YASARA, www.yasara.org

References

1. Philippakis, A.A., Azzariti, D.R., Beltran, S., Brookes, A.J., Brownstein, C.A., Brudno, M., Brunner, H.G., Buske, O.J., Carey, K., Doll, C., et al. (2015). The Matchmaker Exchange: A platform for rare disease gene discovery. Hum. Mutat. *36*, 915–921.

2. Sobreira, N., Schiettecatte, F., Valle, D., and Hamosh, A. (2015). GeneMatcher: A matching tool for connecting investigators with an interest in the same gene. Hum. Mutat. *36*, 928–930.

3. Fritzen, D., Kuechler, A., Grimmel, M., Becker, J., Peters, S., Sturm, M., Hundertmark, H., Schmidt, A., Kreiß, M., Strom, T.M., et al. (2018). De novo FBXO11 mutations are associated with intellectual disability and behavioural anomalies. Hum. Genet. *137*, 401–411.

4. Gregor, A., Sadleir, L.G., Asadollahi, R., Azzarello-Burri, S., Battaglia, A., Ousager, L.B., Boonsawat, P., Bruel, A.L., Buchert, R., Calpena, E., et al.; University of Washington Center for Mendelian Genomics; and DDD Study (2018). De novo variants in the F-box protein FBXO11 in 20 individuals with a variable neurodevelopmental disorder. Am. J. Hum. Genet. *103*, 305–316.

5. Jansen, S., van der Werf, I.M., Innes, A.M., Afenjar, A., Agrawal, P.B., Anderson, I.J., Atwal, P.S., van Binsbergen, E., van den Boogaard, M.J., Castiglia, L., et al. (2019). De novo variants in FBXO11 cause a syndromic form of intellectual disability with behavioral problems and dysmorphisms. Eur. J. Hum. Genet. *27*, 738–746.

6. Martinelli, S., Krumbach, O.H.F., Pantaleoni, F., Coppola, S., Amin, E., Pannone, L., Nouri, K., Farina, L., Dvorsky, R., Lepri, F., et al.; University of Washington Center for Mendelian Genomics (2018). Functional dysregulation of CDC42 causes diverse developmental phenotypes. Am. J. Hum. Genet. *102*, 309–320.

7. Reijnders, M.R.F., Ansor, N.M., Kousi, M., Yue, W.W., Tan, P.L., Clarkson, K., Clayton-Smith, J., Corning, K., Jones, J.R., Lam, W.W.K., et al.; Deciphering Developmental Disorders Study (2017). RAC1 missense mutations in developmental disorders with diverse phenotypes. Am. J. Hum. Genet. *101*, 466–477.

8. Koolen, D.A., Herbergs, J., Veltman, J.A., Pfundt, R., van Bokhoven, H., Stroink, H., Sistermans, E.A., Brunner, H.G., Geurts van Kessel, A., and de Vries, B.B. (2006). Holoprosencephaly and preaxial polydactyly associated with a 1.24 Mb duplication encompassing FBXW11 at 5q35.1. J. Hum. Genet. *51*, 721–726.

9. Li, C.F., Angione, K., and Milunsky, J.M. (2015). Identification of critical region responsible for split hand/foot malformation type 3 (SHFM3) phenotype through systematic review of literature and mapping of breakpoints using microarray data. Microarrays (Basel) *5*, E2.

10. Nusse, R., and Clevers, H. (2017). Wnt/β-catenin signaling, disease, and emerging therapeutic modalities. Cell *169*, 985–999.

11. Fuchs, S.Y., Chen, A., Xiong, Y., Pan, Z.Q., and Ronai, Z. (1999). HOS, a human homolog of Slimb, forms an SCF complex with Skp1 and Cullin1 and targets the phosphorylation-dependent degradation of IkappaB and beta-catenin. Oncogene *18*, 2039–2046.

12. Fujimura, N. (2016). WNT/β-catenin signaling in vertebrate eye development. Front. Cell Dev. Biol. *4*, 138.

13. Noelanders, R., and Vleminckx, K. (2017). How Wnt signaling builds the brain: Bridging development and disease. Neuroscientist *23*, 314–329.

14. Raspopovic, J., Marcon, L., Russo, L., and Sharpe, J. (2014). Modeling digits. Digit patterning is controlled by a Bmp-Sox9-Wnt Turing network modulated by morphogen gradients. Science *345*, 566–570.

15. Cavodeassi, F., Creuzet, S., and Etchevers, H.C. (2018). The hedgehog pathway and ocular developmental anomalies. Hum. Genet., Epub ahead of print.

16. Al-Qattan, M.M. (2018). Zone of polarizing activity regulatory sequence mutations/duplications with preaxial polydactyly and longitudinal preaxial ray deficiency in the phenotype: A review of human cases, animal models, and insights regarding the pathogenesis. BioMed Res. Int. *2018*, 1573871.

17. Fantes, J., Ragge, N.K., Lynch, S.A., McGill, N.I., Collin, J.R., Howard-Peebles, P.N., Hayward, C., Vivian, A.J., Williamson, K., van Heyningen, V., and FitzPatrick, D.R. (2003). Mutations in SOX2 cause anophthalmia. Nat. Genet. *33*, 461–463.

18. Errichiello, E., Gorgone, C., Giuliano, L., Iadarola, B., Cosentino, E., Rossato, M., Kurtas, N.E., Delledonne, M., Mattina, T., and Zuffardi, O. (2018). SOX2: Not always eye malformations. Severe genital but no major ocular anomalies in a female patient with the recurrent c.70del20 variant. Eur. J. Med. Genet. *61*, 335–340.

19. Jin, J., Cardozo, T., Lovering, R.C., Elledge, S.J., Pagano, M., and Harper, J.W. (2004). Systematic analysis and nomenclature of mammalian F-box proteins. Genes Dev. *18*, 2573–2580.

20. Wu, G., Xu, G., Schulman, B.A., Jeffrey, P.D., Harper, J.W., and Pavletich, N.P. (2003). Structure of a beta-TrCP1-Skp1-beta-catenin complex: Destruction motif binding and lysine specificity of the SCF(beta-TrCP1) ubiquitin ligase. Mol. Cell *11*, 1445–1456.

21. Xu, C., and Min, J. (2011). Structure and function of WD40 domain proteins. Protein Cell *2*, 202–214.

22. El-Hattab, A.W., Dai, H., Almannai, M., Wang, J., Faqeih, E.A., Al Asmari, A., Saleh, M.A.M., Elamin, M.A.O., Alfadhel, M., Alkuraya, F.S., et al. (2017). Molecular and clinical spectra of FBXL4 deficiency. Hum. Mutat. *38*, 1649–1659.

23. Willems, A.R., Schwab, M., and Tyers, M. (2004). A hitchhiker's guide to the cullin ubiquitin ligases: SCF and its kin. Biochim. Biophys. Acta *1695*, 133–170.

24. Petrovski, S., Wang, Q., Heinzen, E.L., Allen, A.S., and Goldstein, D.B. (2013). Genic intolerance to functional variation and the interpretation of personal genomes. PLoS Genet. *9*, e1003709.

25. Samocha, K.E., Robinson, E.B., Sanders, S.J., Stevens, C., Sabo, A., McGrath, L.M., Kosmicki, J.A., Rehnström, K., Mallick, S., Kirby, A., et al. (2014). A framework for the interpretation of de novo mutation in human disease. Nat. Genet. *46*, 944–950.

26. Lek, M., Karczewski, K.J., Minikel, E.V., Samocha, K.E., Banks, E., Fennell, T., O'Donnell-Luria, A.H., Ware, J.S., Hill, A.J., Cummings, B.B., et al.; Exome Aggregation Consortium (2016). Analysis of protein-coding genetic variation in 60,706 humans. Nature *536*, 285–291.

27. De Rubeis, S., He, X., Goldberg, A.P., Poultney, C.S., Samocha, K., Cicek, A.E., Kou, Y., Liu, L., Fromer, M., Walker, S., et al.; DDD Study; Homozygosity Mapping Collaborative for Autism; and UK10K Consortium (2014). Synaptic, transcriptional and chromatin genes disrupted in autism. Nature *515*, 209–215.

28. Iossifov, I., O'Roak, B.J., Sanders, S.J., Ronemus, M., Krumm, N., Levy, D., Stessman, H.A., Witherspoon, K.T., Vives, L., Patterson, K.E., et al. (2014). The contribution of de novo coding mutations to autism spectrum disorder. Nature *515*, 216–221.

29. Cooper, G.M., Stone, E.A., Asimenos, G., Green, E.D., Batzoglou, S., Sidow, A.; and NISC Comparative Sequencing Program (2005). Distribution and intensity of constraint in mammalian genomic sequence. Genome Res. *15*, 901–913.

30. Davydov, E.V., Goode, D.L., Sirota, M., Cooper, G.M., Sidow, A., and Batzoglou, S. (2010). Identifying a high fraction of the human genome to be under selective constraint using GERP++. PLoS Comput. Biol. *6*, e1001025.

31. Havrilla, J.M., Pedersen, B.S., Layer, R.M., and Quinlan, A.R. (2019). A map of constrained coding regions in the human genome. Nat. Genet. *51*, 88–95.

32. Berman, H.M., Westbrook, J., Feng, Z., Gilliland, G., Bhat, T.N., Weissig, H., Shindyalov, I.N., and Bourne, P.E. (2000). The Protein Data Bank. Nucleic Acids Res. *28*, 235–242.

33. Motta, M., Fidan, M., Bellacchio, E., Pantaleoni, F., Schneider-Heieck, K., Coppola, S., Borck, G., Salviati, L., Zenker, M., Cirstea, I.C., et al. (2019). Dominant Noonan syndrome-causing LZTR1 mutations specifically affect the kelch domain substrate-recognition surface and enhance RAS-MAPK signaling. Hum. Mol. Genet *28*, 1007–1022.

34. Lelieveld, S.H., Wiel, L., Venselaar, H., Pfundt, R., Vriend, G., Veltman, J.A., Brunner, H.G., Vissers, L.E.L.M., and Gilissen, C. (2017). Spatial clustering of de novo missense mutations identifies candidate neurodevelopmental disorder-associated genes. Am. J. Hum. Genet. *101*, 478–484.

35. Schymkowitz, J., Borg, J., Stricher, F., Nys, R., Rousseau, F., and Serrano, L. (2005). The FoldX web server: An online force field. Nucleic Acids Res. *33*, W382-8.

36. Lai, C.S., Gerrelli, D., Monaco, A.P., Fisher, S.E., and Copp, A.J. (2003). FOXP2 expression during brain development coincides with adult sites of pathology in a severe speech and language disorder. Brain *126*, 2455–2462.

37. Morais da Silva, S., Hacker, A., Harley, V., Goodfellow, P., Swain, A., and Lovell-Badge, R. (1996). Sox9 expression during gonadal development implies a conserved role for the gene in testis differentiation in mammals and birds. Nat. Genet. *14*, 62–68.

38. Hooper, J.E., and Scott, M.P. (2005). Communicating with Hedgehogs. Nat. Rev. Mol. Cell Biol. *6*, 306–317.

39. Aldinger, K.A., Mendelsohn, N.J., Chung, B.H., Zhang, W., Cohn, D.H., Fernandez, B., Alkuraya, F.S., Dobyns, W.B., and Curry, C.J. (2016). Variable brain phenotype primarily affects the brainstem and cerebellum in patients with osteogenesis imperfecta caused by recessive WNT1 mutations. J. Med. Genet. *53*, 427–430.

40. Thisse, C., and Thisse, B. (2008). High-resolution in situ hybridization to whole-mount zebrafish embryos. Nat. Protoc. *3*, 59–69.

41. El-Brolosy, M.A., Kontarakis, Z., Rossi, A., Kuenne, C., Günther, S., Fukuda, N., Kikhi, K., Boezio, G.L.M., Takacs, C.M., Lai, S.L., et al. (2019). Genetic compensation triggered by mutant mRNA degradation. Nature *568*, 193–197.

42. El-Brolosy, M.A., and Stainier, D.Y.R. (2017). Genetic compensation: A phenomenon in search of mechanisms. PLoS Genet. *13*, e1006780.

43. Rossi, A., Kontarakis, Z., Gerri, C., Nolte, H., Hölper, S., Krüger, M., and Stainier, D.Y. (2015). Genetic compensation induced by deleterious mutations but not gene knockdowns. Nature *524*, 230–233.

44. Aberle, H., Bauer, A., Stappert, J., Kispert, A., and Kemler, R. (1997). beta-catenin is a target for the ubiquitin-proteasome pathway. EMBO J. *16*, 3797–3804.

45. Kim, C.H., Oda, T., Itoh, M., Jiang, D., Artinger, K.B., Chandrasekharappa, S.C., Driever, W., and Chitnis, A.B. (2000). Repressor activity of Headless/Tcf3 is essential for vertebrate head formation. Nature *407*, 913–916.

46. Heisenberg, C.P., Houart, C., Take-Uchi, M., Rauch, G.J., Young, N., Coutinho, P., Masai, I., Caneparo, L., Concha, M.L., Geisler, R., et al. (2001). A mutation in the Gsk3-binding domain of zebrafish Masterblind/Axin1 leads to a fate transformation of telencephalon and eyes to diencephalon. Genes Dev. *15*, 1427–1434.

47. Young, R.M., Hawkins, T.A., Cavodeassi, F., Stickney, H.L., Schwarz, Q., Lawrence, L.M., Wierzbicki, C., Cheng, B.Y., Luo, J., Ambrosio, E.M., et al. (2019). Compensatory growth renders Tcf7l1a dispensable for eye formation despite its requirement in eye field specification. eLife *8*, e40093.

48. Hurlstone, A.F., Haramis, A.P., Wienholds, E., Begthel, H., Korving, J., Van Eeden, F., Cuppen, E., Zivkovic, D., Plasterk, R.H., and Clevers, H. (2003). The Wnt/beta-catenin pathway regulates cardiac valve formation. Nature *425*, 633–637.

49. Kennerson, M.L., Warburton, T., Nelis, E., Brewer, M., Polly, P., De Jonghe, P., Timmerman, V., and Nicholson, G.A. (2007). Mutation scanning the GJB1 gene with high-resolution melting analysis: implications for mutation scanning of genes for Charcot-Marie-Tooth disease. Clin. Chem. *53*, 349–352.

50. Stamos, J.L., and Weis, W.I. (2013). The β-catenin destruction complex. Cold Spring Harb. Perspect. Biol. *5*, a007898.

51. Winston, J.T., Strack, P., Beer-Romero, P., Chu, C.Y., Elledge, S.J., and Harper, J.W. (1999). The SCFbeta-TRCP-ubiquitin ligase complex associates specifically with phosphorylated destruction motifs in IkappaBalpha and beta-catenin and stimulates IkappaBalpha ubiquitination in vitro. Genes Dev. *13*, 270–283.

52. Li, Y., Pawlik, B., Elcioglu, N., Aglan, M., Kayserili, H., Yigit, G., Percin, F., Goodman, F., Nürnberg, G., Cenani, A., et al. (2010). LRP4 mutations alter Wnt/beta-catenin signaling and cause limb and kidney malformations in Cenani-Lenz syndrome. Am. J. Hum. Genet. *86*, 696–706.

53. Hoseth, E.Z., Krull, F., Dieset, I., Mørch, R.H., Hope, S., Gardsjord, E.S., Steen, N.E., Melle, I., Brattbakk, H.R., Steen, V.M., et al. (2018). Exploring the Wnt signaling pathway in schizophrenia and bipolar disorder. Transl. Psychiatry *8*, 55.

54. Martinez, G., Wijesinghe, M., Turner, K., Abud, H.E., Taketo, M.M., Noda, T., Robinson, M.L., and de Iongh, R.U. (2009). Conditional mutations of beta-catenin and APC reveal roles for canonical Wnt signaling in lens differentiation. Invest. Ophthalmol. Vis. Sci. *50*, 4794–4806.

55. Alldredge, A., and Fuhrmann, S. (2016). Loss of Axin2 causes ocular defects during mouse eye development. Invest. Ophthalmol. Vis. Sci. *57*, 5253–5262.

56. Carter, T.C., Sicko, R.J., Kay, D.M., Browne, M.L., Romitti, P.A., Edmunds, Z.L., Liu, A., Fan, R., Druschel, C.M., Caggana, M., et al. (2017). Copy-number variants and candidate gene mutations in isolated split hand/foot malformation. J. Hum. Genet. *62*, 877–884.

57. Jiang, J., and Struhl, G. (1998). Regulation of the Hedgehog and Wingless signalling pathways by the F-box/WD40-repeat protein Slimb. Nature *391*, 493–496.

58. Milétich, I., and Limbourg-Bouchon, B. (2000). Drosophila null slimb clones transiently deregulate Hedgehog-independent transcription of wingless in all limb discs, and induce decapentaplegic transcription linked to imaginal disc regeneration. Mech. Dev. *93*, 15–26.

59. Skwarek, L.C., Windler, S.L., de Vreede, G., Rogers, G.C., and Bilder, D. (2014). The F-box protein Slmb restricts the activity of aPKC to polarize epithelial cells. Development *141*, 2978–2983.

60. Johnson, D.R. (1967). Extra-toes: A new mutant gene causing multiple abnormalities in the mouse. J. Embryol. Exp. Morphol. *17*, 543–581.

61. Franz, T., and Besecke, A. (1991). The development of the eye in homozygotes of the mouse mutant Extra-toes. Anat. Embryol. (Berl.) *184*, 355–361.

62. Furimsky, M., and Wallace, V.A. (2006). Complementary Gli activity mediates early patterning of the mouse visual system. Dev. Dyn. *235*, 594–605.

63. Hui, C.C., and Joyner, A.L. (1993). A mouse model of greig cephalopolysyndactyly syndrome: The extra-toesJ mutation contains an intragenic deletion of the Gli3 gene. Nat. Genet. *3*, 241–246.

64. Bakrania, P., Efthymiou, M., Klein, J.C., Salt, A., Bunyan, D.J., Wyatt, A., Ponting, C.P., Martin, A., Williams, S., Lindley, V.,

et al. (2008). Mutations in BMP4 cause eye, brain, and digit developmental anomalies: Overlap between the BMP4 and hedgehog signaling pathways. Am. J. Hum. Genet. *82*, 304–319.

65. Bakrania, P., Ugur Iseri, S.A., Wyatt, A.W., Bunyan, D.J., Lam, W.W., Salt, A., Ramsay, J., Robinson, D.O., and Ragge, N.K. (2010). Sonic hedgehog mutations are an uncommon cause of developmental eye anomalies. Am. J. Med. Genet. A. *152A*, 1310–1313.

66. Chassaing, N., Davis, E.E., McKnight, K.L., Niederriter, A.R., Causse, A., David, V., Desmaison, A., Lamarre, S., Vincent-Delorme, C., Pasquier, L., et al. (2016). Targeted resequencing identifies PTCH1 as a major contributor to ocular developmental anomalies and extends the SOX2 regulatory network. Genome Res. *26*, 474–485.

67. Roessler, E., Du, Y.Z., Mullor, J.L., Casas, E., Allen, W.P., Gillessen-Kaesbach, G., Roeder, E.R., Ming, J.E., Ruiz i Altaba, A., and Muenke, M. (2003). Loss-of-function mutations in the human GLI2 gene are associated with pituitary anomalies and holoprosencephaly-like features. Proc. Natl. Acad. Sci. USA *100*, 13424–13429.

68. Rahimov, F., Ribeiro, L.A., de Miranda, E., Richieri-Costa, A., and Murray, J.C. (2006). GLI2 mutations in four Brazilian patients: How wide is the phenotypic spectrum? Am. J. Med. Genet. A. *140*, 2571–2576.

69. Johnston, J.J., Sapp, J.C., Turner, J.T., Amor, D., Aftimos, S., Aleck, K.A., Bocian, M., Bodurtha, J.N., Cox, G.F., Curry, C.J., et al. (2010). Molecular analysis expands the spectrum of phenotypes associated with GLI3 mutations. Hum. Mutat. *31*, 1142–1154.

70. Bertolacini, C.D.P., Ribeiro-Bicudo, L.A., Petrin, A., Richieri-Costa, A., and Murray, J.C. (2012). Clinical findings in patients with GLI2 mutations–phenotypic variability. Clin. Genet. *81*, 70–75.

71. Roberts, A.E., Allanson, J.E., Tartaglia, M., and Gelb, B.D. (2013). Noonan syndrome. Lancet *381*, 333–342.

72. Tartaglia, M., and Gelb, B.D. (2010). Disorders of dysregulated signal traffic through the RAS-MAPK pathway: Phenotypic spectrum and molecular mechanisms. Ann. N Y Acad. Sci. *1214*, 99–121.

73. de la Vega, M., Burrows, J.F., and Johnston, J.A. (2011). Ubiquitination: Added complexity in Ras and Rho family GTPase function. Small GTPases *2*, 192–201.

74. Steklov, M., Pandolfi, S., Baietti, M.F., Batiuk, A., Carai, P., Najm, P., Zhang, M., Jang, H., Renzi, F., Cai, Y., et al. (2018). Mutations in LZTR1 drive human disease by dysregulating RAS ubiquitination. Science *362*, 1177–1182.

75. Bigenzahn, J.W., Collu, G.M., Kartnig, F., Pieraks, M., Vladimer, G.I., Heinz, L.X., Sedlyarov, V., Schischlik, F., Fauster, A., Rebsamen, M., et al. (2018). LZTR1 is a regulator of RAS ubiquitination and signaling. Science *362*, 1171–1177.

76. Kim, S.E., Yoon, J.Y., Jeong, W.J., Jeon, S.H., Park, Y., Yoon, J.B., Park, Y.N., Kim, H., and Choi, K.Y. (2009). H-Ras is degraded by Wnt/beta-catenin signaling via beta-TrCP-mediated polyubiquitylation. J. Cell Sci. *122*, 842–848.

77. Li, Q., and Wang, K. (2017). InterVar: Clinical interpretation of genetic variants by the 2015 ACMG-AMP guidelines. Am. J. Hum. Genet. *100*, 267–280.

78. Ng, P.C., and Henikoff, S. (2003). SIFT: Predicting amino acid changes that affect protein function. Nucleic Acids Res. *31*, 3812–3814.

79. Adzhubei, I.A., Schmidt, S., Peshkin, L., Ramensky, V.E., Gerasimova, A., Bork, P., Kondrashov, A.S., and Sunyaev, S.R. (2010). A method and server for predicting damaging missense mutations. Nat. Methods *7*, 248–249.